ELSEVIER Science Press
Available online at www.sciencedirect.com
ScienceDirect
Trans. Nonferrous Met. Soc. China 33(2023) 2559−2573
Transactions of Nonferrous Metals Society of China
www.tnmsc.cn

Sn-induced phase transformation mechanism from θ' to θ in Al−4Cu alloy and its influence on high temperature strength

Guang-jing LI, Xing-hui PAN, Heng-cheng LIAO, Ji-wei ZHENG, Mo-tong YANG, Long-jie QIAN, Li-zhen LU

Jiangsu Key Laboratory of Advanced Metallic Materials,
School of Materials Science and Engineering, Southeast University, Nanjing 211189, China

Received 15 March 2022; accepted 14 June 2022

Abstract: The effects of 0.02 wt.% Sn addition to Al−4Cu alloy on the phase transformation mechanism from θ' to θ phase during a long-time heat exposure at 573 K for 100 h and on high temperature strength were studied through microstructure observation and tensile test. It is found that Sn micro-alloying in Al−4Cu alloy completely changes the mechanism of $\theta' \rightarrow \theta$ phase transformation during the long-time heat exposure. In the alloy without Sn addition, rod-like θ phase nucleates and grows on the surface of coarsened disc-like θ' phase. However, with Sn-micro-alloying, θ phase firstly heterogeneously nucleates on β-Sn particles, and then grows into much coarser needle-like phase. Trace addition of Sn significantly increases the yield strength of T5-samples at both room temperature and 573 K, because addition of Sn increases the number density of θ' particles and reduces its size. But, after the long-time heat exposure, the high temperature (573 K) strength of Al−4Cu alloy is severely degraded because Sn accelerates the phase transformation from θ' to θ phase.

Key words: Sn; Al−Cu alloy; θ phase; long-time heat exposure; phase transformation; high temperature strength

1 Introduction

Aluminum alloys have been widely applied in various industries, especially in transportation and aerospace industries, because of their good strength, low density and excellent castability [1]. Al−Cu system alloy is one of the best candidates for applications at high temperatures. Its strength can be significantly improved by the precipitation hardening from very fine metastable particles. The main precipitation hardening phases in this system are well known as GP I zone (pre-θ''), θ'' (Al_3Cu, GP II zone) and θ' (Al_2Cu) [2−4]. θ (Al_2Cu) phase is the final equilibrium state of the aforementioned meta-stable ageing-precipitates. Due to the high number density, fine size and coherent/semi-coherent relationships with Al matrix, θ'' and θ' meta-stable precipitates are the favorable ones that can significantly strengthen the alloy [3,5]. Both θ'' and θ' precipitates have tetragonal structure and lattice constants of $a=b=0.405$ nm, $c=0.768$ nm for θ'' phase and $a=b=0.404$ nm, $c=0.580$ nm for θ' phase [6,7]. θ phase has a tetragonal structure too, with lattice constants of $a=b=0.605$ nm, and $c=0.487$ nm [7,8]. The structure of Al matrix is face-centered-cubic and its lattice constant is $a=0.404$ nm [9]. But the contribution of the equilibrium θ-Al_2Cu precipitate to the strength is usually thought to be very low even harmful, because it loses the coherent relationship with the matrix and always has a larger size [2,10]. Thus, almost all studies on precipitation strengthening in Al−Cu and Al−Si−Cu alloys are focused on the precipitation behaviors of θ'' and θ'.

Most research works about θ'' and θ' precipitates in Al−Cu alloys are focused on the strengthening mechanisms [3], formation and

---

Corresponding author: Heng-cheng LIAO, Tel: +86-25-52090686, E-mail: hengchengliao@seu.edu.cn

DOI: 10.1016/S1003-6326(23)66281-8

growth mechanisms [11−14] and refinement mechanism [15,16] of these precipitates. Using micropillar-compression-tests, BELLÓN et al [3] confirmed that the strengthening mechanisms of θ'' and θ' precipitates in Al−4wt.%Cu alloy are dislocation-cutting and dislocation-bypassing mechanisms, respectively. There are two mechanisms about the formation of θ' precipitates: transformation from θ'' precipitates [17] and nucleation directly from the matrix [18]. BOURGEOIS et al [19] found that there is a transition layer (about 1 nm) at the α/θ' interface, which contains two structure phases: θ'' and θ'_t ($Al_{11}Cu_7$, with the ordered superlattice of θ' phase). This further indicates that the formation and growth of θ' precipitates in α(Al) matrix are closely related to the θ'' phase. This transformation mechanism is also connected to the existence of vacancies [13]. In addition, some studies reported that the formation of θ' precipitates can skip θ'' phase, and they directly nucleate on dislocations [20] or on pre-existed β-Sn particles [16]. But for θ phase, there are few reports for its transformation mechanism, because it is always thought that the existence of θ phase in Al−Cu and Al−Si−Cu alloys should be avoided as much as possible.

Heat-resistance is one of the outstanding advantages of Al−Cu or Al−Si−Cu alloys. Many studies are focused on improving the thermal-stability of θ' precipitates and on the corresponding impact on the strength at high temperatures. For example, researchers in Refs. [10,21−23] reported that Mn, Zr and Sc can improve the thermal-stability of θ' precipitates by forming an interface layer between α(Al) and θ' phase. This layer is composed of low diffusion coefficient atoms that can hinder atomic diffusion of Cu solute during the growth of θ' phase. However, heat-resistant components made of Al−Cu or Al−Si−Cu alloys always work at high temperature for a much long time exposure. Thus, the phase transformation of $\theta' \rightarrow \theta$ and its effect on high temperature strength should be taken into account. However, reports on it are very few.

The effect of Sn addition on the ageing precipitation behavior of Al−Cu alloy was first reported by SULLY et al [24] in 1949, where trace addition of Sn can significantly change the precipitation behavior of Al−Cu alloy, increasing the hardness and shortening the peak aging time. Since then, many similar studies on Al−Cu and Al−Mg−Si alloys have been reported. The precipitation of θ' or β'' phases could be promoted by Sn addition, because the prior formation of β-Sn particles ($I41/amd$, a=0.583 nm, c=0.318 nm [25]) could act as the heterogeneous nucleation substrates for θ' [16,26] or β'' phases [27], or Sn addition could increase the number density of vacancies that could accelerate the diffusion rate of solute atoms [9]. However, there are no studies on the effect of trace addition of Sn on the evolution of the ageing precipitates in Al−Cu alloy during a subsequent long-time exposure at high temperatures, especially on the transformation mechanism of $\theta' \rightarrow \theta$.

Thus, in this study, the evolution of ageing precipitates in Al−4Cu alloy (with/without trace addition of Sn) during a short-time/long-time heat exposure was observed by TEM/HRTEM and the mechanism of $\theta' \rightarrow \theta$ phase transformation was discussed in details. The effect of the evolution of ageing precipitates on high temperature mechanical properties was evaluated too.

2 Experimental

2.1 Alloy preparation

The studied alloys (A4C alloy: Al−4wt.%Cu; A4C−S alloy: Al−4wt.%Cu−0.02wt.%Sn) were prepared by the same method as described in Ref. [28]. Besides, trace Sn was added into the A4C alloy melt in the form of Al−10wt.%Sn master alloy. The main chemical composition of the A4C and A4C−S alloys was measured by spark emission spectrometer (MAXx LMF15) as: Al−4.06wt.%Cu and Al−4.07wt.%Cu−0.019wt.%Sn.

The obtained plate-like castings were solutionized at 788 K for 5 h and 848 K for 3 h, then quenched in water (abbreviated as T4 state), and subsequently aged at 438 K for 5 h (an under-ageing heat treatment, abbreviated as T5 state). In order to study the effect of Sn on the phase transformation mechanism from θ' to θ, the evolution of ageing precipitates and high temperature strength, some samples experienced a short-time/long-time heat exposure (exposed at 573 K for 0.5 h (STHE treatment) and for 100 h (LTHE treatment), respectively, and then cooled in air to room temperature).

2.2 Microstructure observation and tensile test

The same instruments and methods as described in Refs. [28,29] were adopted to carry out the microstructure observation and tensile test of the studied alloys. The yield strength (here, $\sigma_{0.2}$, obtained by CMT5105 with a rate of 1 mm/min) was used to evaluate the strengthening effect from the microstructure evolution. To reduce the accidental error, an average value of strength was taken from 3 replicates.

3 Results

3.1 Microstructure evolution in as-cast, T4 and T5 states

Due to trace addition of Sn (only 0.019 wt.%) to Al−4Cu alloy, there are no considerable differences observed in the microstructure of the A4C and A4C−S alloys in as-cast and T4 states, as shown in Fig. 1. However, in T5 state, the microstructure of the A4C−S alloy is greatly different from that of the A4C alloy.

TEM bright field images in Figs. 2(a) and (c) show the ageing precipitates in the matrix of the studied A4C and A4C−S alloys in T5 state, respectively. Trace addition of Sn to Al−4Cu alloy can significantly affect the ageing precipitation of metastable particles. For A4C alloy in T5 state, all ageing precipitation particles in Fig. 2(a) are θ'' phase, with a length of about 50 nm and a thickness of about 1 nm. It is confirmed by SAED pattern in Fig. 2(b) that the fine streaks are the typical feature of θ'' phase in aluminum solution [20,30]. However, for A4C−S alloy in T5 state, besides the fine θ'' particles (about 2 nm in thickness), a great number of coarse precipitation particles (with a thickness of about 4 nm) are observed, as seen in Fig. 2(c). SAED pattern of the region containing these particles is illustrated in Fig. 2(d). Besides those fine streaks, weak spots are observed (the typical feature of θ' phase in Al solution [20,31]), confirming that θ' particles have been precipitated. That is to say, Sn micro-alloying accelerates the formation of θ' phase during the ageing treatment, in accordance with the results in Ref. [16]. After the same solution and ageing treatments as for the A4C alloy, θ' phase coexists with θ'' phase in the matrix of the A4C−S alloy. It should be noted that the needle-like shape of these precipitates is the semi-coherent of disc-like θ'' and θ' phases observed from [001] and $[0\bar{1}1]$ axes of Al matrix.

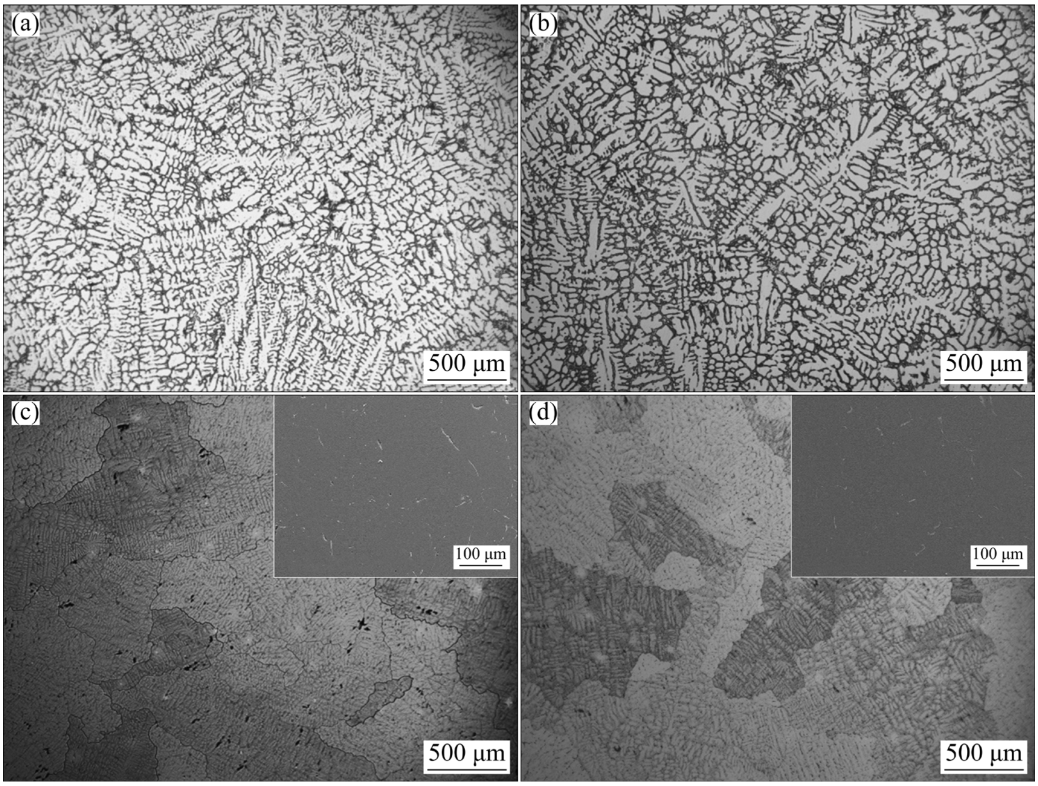

Fig. 1 Microstructure of A4C (a, c) and A4C−S (b, d) alloys in as-cast (a, b) and T4 (c, d) states

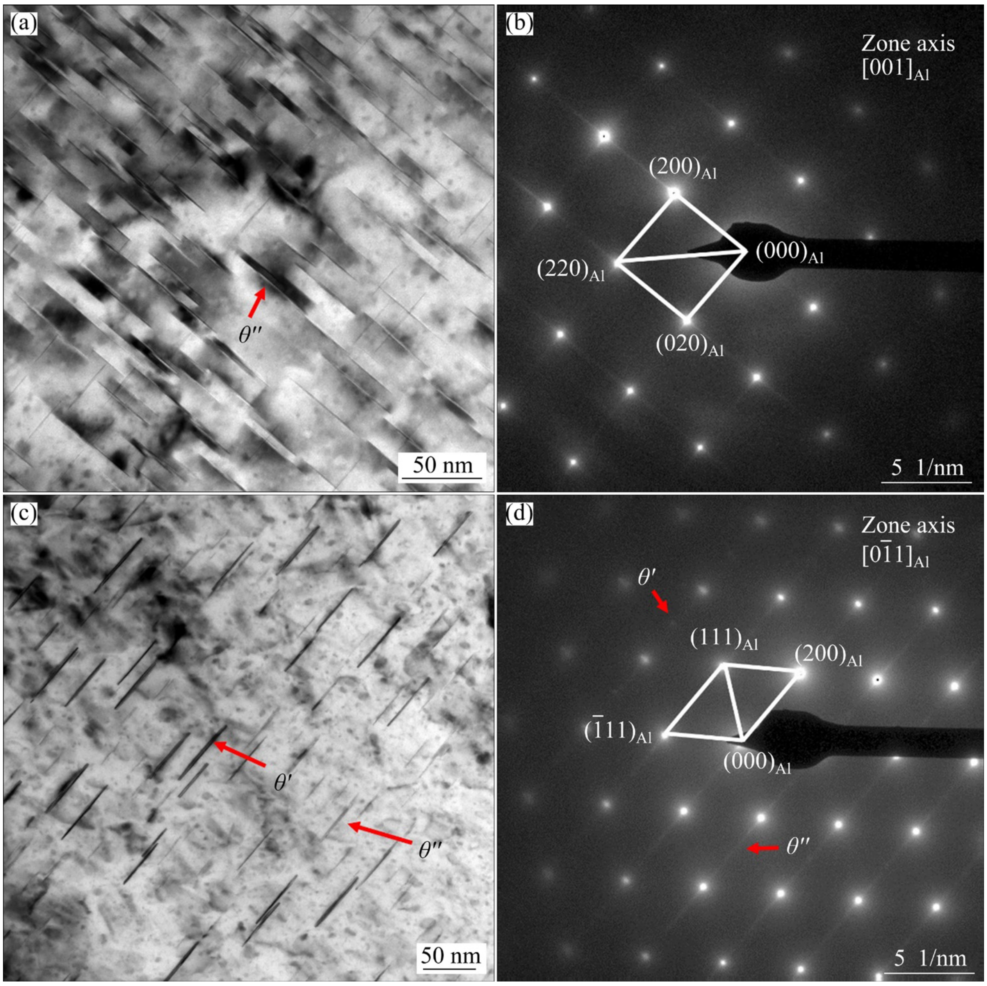

Fig. 2 TEM bright field images showing precipitates in Al matrix of A4C (a) and A4C−S (c) alloys in T5 state, and corresponding SAED patterns of zones containing these precipitation particles in A4C (b) and A4C−S (d) alloys

3.2 Microstructure evolution during long-time heat exposure in T5 state

TEM bright images in Figs. 3(a−c) illustrate the evolution of the ageing precipitates in the matrix of A4C alloy (in T5 state) after a long-time heat exposure at 573 K for 100 h (LTHE treatment). Compared with that in Fig. 2(a), the ageing precipitation particles are significantly coarsened (about 1 μm in length and 30 nm in thickness). From the high magnification images (Figs. 3(b) and (c)), it is interesting to note that most of the coarsened needles seem to have a sandwich structure. SAED patterns in Figs. 3(d−f) reveal different structures in different regions of a coarse needle in Fig. 3(b). SAED pattern of Zone *A* is regular (Fig. 3(d)), similar to the normal SAED patterns of θ′ phase shown in Refs. [20,31], where the weaker spots between the stronger spots of Al solution represent the existence of θ′ phase. Thus, Zone *A* in the needle is θ′ phase. Figure 3(f) illustrates SAED pattern of Zone *C* (the end of coarse needle). Definitely, there are two sets of spots. One belongs to θ phase and the other belongs to Al matrix around θ phase. This indicates that the end of this needle has transformed into θ phase. In Zone *B*, the diffraction spots are disorderly (Fig. 3(e)); however, the spots belonging to θ′ and θ phases can be discernibly observed. It indicates that this part is at the transition stage of phase tranformation from θ′ to θ.

After the LTHE treatment, the morphology of precipitates in the matrix of A4C−S alloy is completely different from that in A4C alloy, as shown in Fig. 4. There are a few very coarse needles with random growth orientations, not like θ″ or θ′ phases observed in T5 state (Fig. 2(c)). A large number of short and small rod-like precipitates are seen too. SAED pattern in Fig. 4(b) suggests the coarse needle-like precipitates (Zone *D* in Fig. 4(a)) are equilibrium *θ* phase. It is well known that *θ* phase has not a coherent/semi-coherent relationship with the matrix like *θ*″ and *θ*′ phases [32]. The formation of *θ* phase will not produce an elastic strain zone in the matrix around *θ* particle that will significantly decrease the strengthening contribution to the matrix. SAED pattern of the region containing the short rod-like particles (Zone *E* in Fig. 4(a)) is shown in Fig. 4(c). To the right of each strong diffraction spot of Al matrix, there is one weak spot. These weak spots usually belong to *θ*′ phase, but, here, they do not locate at the line of two adjacent spots of Al matrix as shown in Fig. 2(d) or in Refs. [20, 31]. Thus, these short and small rod-like *θ*′ precipitates are thought to be a variant of *θ*′ phase (similar to shape with normal *θ*′ phase, here, named as *θ*′-like particle) that loses the coherent orientation relationship with Al matrix. Unlike those in the A4C alloy, *θ*′ particles observed in A4C−S alloy are not coarsened after the LTHE treatment, and conversely are shrunk to great extent (compared the small rod-like particles in Fig. 4(a) with those in Figs. 3(a−c)). They experienced a coarsening course (demonstrated by TEM observation of the sample in STHE state) but are

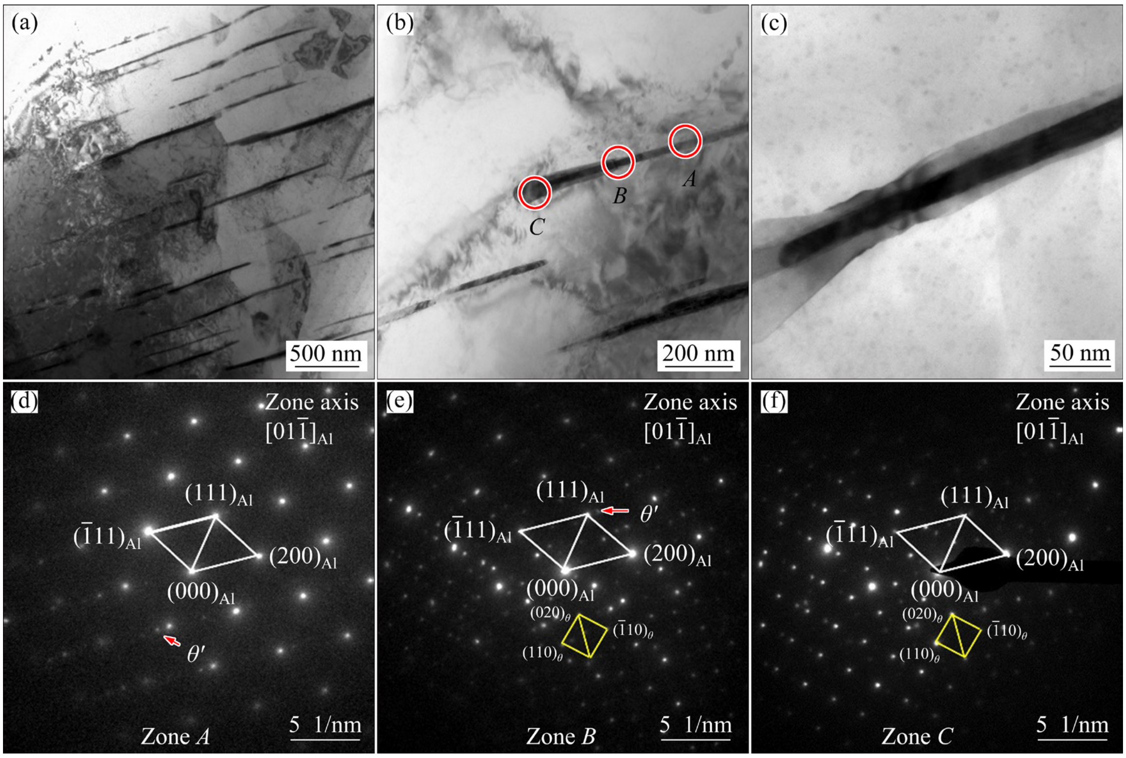

Fig. 3 TEM bright field images showing precipitates in matrix of A4C alloy in T5 state after LTHE treatment (a−c) and its SAED patterns corresponding to Zones *A* (d), *B* (e) and *C* (f) in (b), respectively

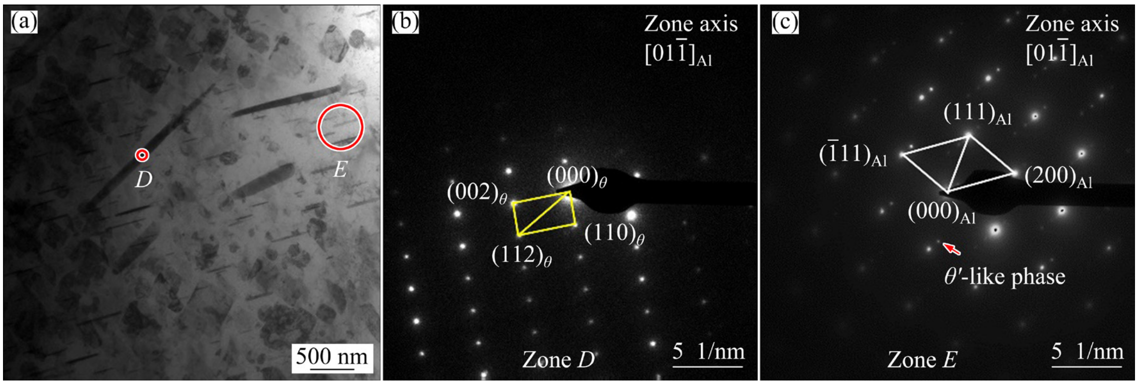

Fig. 4 TEM bright field image showing precipitates in matrix of A4C−S alloy in T5 state after LTHE treatment (a) and its SAED patterns corresponding to Zones *D* (b) and *E* (c) in (a), respectively

shrunk finally due to the re-dissolving of Cu atoms into the matrix during the phase transformation from θ' to θ.

It is interesting to note that the surface of these small rods is very smooth, and no film-like θ phase is formed on the surface as seen in Fig. 3(c). The above results indicate that the existence of Sn in A4C−S alloy changes the phase transformation mode from θ' to θ during the LTHE treatment.

3.3 Variation of yield strength

Figure 5 shows the representative tensile engineering stress−strain curves of the studied A4C and A4C−S alloys in T5 state and after a subsequent LTHE treatment. Table 1 summarized the tensile yield strength ($\sigma_{0.2}$) at RT (room temperature) and HT (high temperature, 573 K). For A4C alloy in T5 state, the room temperature yield strength is 159 MPa, which is mainly from the strengthening effect of θ'' precipitation particles in under-aged state. However, when the test temperature was increased to 573 K, $\sigma_{0.2}$ of A4C alloy is remarkably decreased to 93 MPa. It is due to the decrease in binding-force between atoms, the accelerated motion of dislocations and the coarsening of precipitation particles at 573 K. After the LTHE treatment, the significant coarsening behavior of θ' precipitates and transformation from θ' to θ are observed in the studied alloys (Figs. 3(a−c)), thus, $\sigma_{0.2}$ of A4C alloy at 573 K is further decreased to 74 MPa. However, for A4C−S alloy, $\sigma_{0.2}$ of the samples in T5 state is significantly increased to 283 MPa at RT and 130 MPa at 573 K, with increments of 124 and 37 MPa compared with A4C alloy, respectively. This indicates that Sn micro-alloying in Al−4Cu alloy can greatly increase $\sigma_{0.2}$ at RT and 573 K of the samples in T5 state. After the LTHE treatment, $\sigma_{0.2}$ at 573 K of A4C−S alloy is decreased to 63 MPa (with a great decrement of 67 MPa), even 11 MPa lower than that of A4C alloy. This implies that, on the one hand, long-time service at high temperature will result in a severe degradation of high temperature strength of the studied Al−Cu alloys. On the other hand, of more importance, a high value of strength obtained by usual tensile test instantaneously at high temperature cannot guarantee a high value of strength after long-time service at high temperature. That is, the strength obtained from usual tensile test at high temperature cannot be well used to evaluate the strength under a long-time high temperature condition.

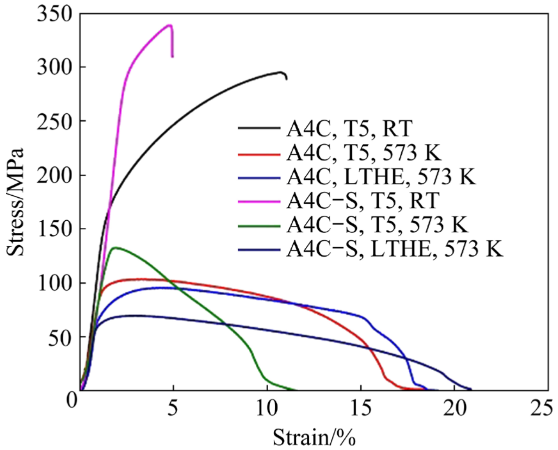

Fig. 5 Representative tensile engineering stress−strain curves of studied alloys in different states at RT and 573 K

Table 1 Data of tensile yield strength ($\sigma_{0.2}$) of studied alloys in different states at RT and 573 K

Alloy	$\sigma_{0.2}$/MPa		
	RT (T5)	573 K (T5)	573 K (T5+(573 K, 100 h))
A4C	159±11	93±4	74±2
A4C−S	283±19	130±5	63±3

4 Discussion

4.1 Effect of Sn-micro-alloying on precipitation of θ' phase

There are two mechanisms that can be used to explain the acceleration effect of trace addition of Sn on the formation of θ' phase during the ageing treatment: vacancy-related and heterogeneous-nucleation-related. As for the vacancy-related mechanism, due to the fact that the atomic radius of Sn is larger than that of Al and Cu atoms, Sn atoms or Sn-rich clusters are more likely to bond with the vacancies to reduce the lattice distortion [27,31]. The bonding energy of Sn atom with vacancy (0.34 eV, calculated by DFT in Ref. [33]) in Al−Cu alloy is much larger than that of Cu atom with vacancy (0.17 eV, calculated by DFT in Ref. [33]). This means that Sn in α(Al) solution of Al−Cu alloy can capture more vacancies during the solution treatment at high temperature. A higher proportion of vacancies can be retained in the α(Al) solution with Sn-micro-alloying after the quenching. A high proportion of vacancies at a lower temperature (such as during the ageing treatment) can decrease the diffusion activation energy of Cu atom in α(Al) solution and thus promote its diffusion [9]. Therefore, during the ageing treatment, the formation or transformation of both θ'' and θ' phases will be accelerated by the existence of Sn solute atoms in α(Al) solution [10,34]. Another mechanism is heterogeneous-nucleation-related. Because the solid solubility of Sn in α(Al) solution is very small, the existence of Sn element in Al−Cu alloy is always in the form of elemental β-Sn particles ($I41/amd$, a=0.583 nm, and c=0.318 nm [25]). The results of HOMMA et al [35] through APT observation indicated that β-Sn phase could rapidly form in the initial stage of ageing treatment because Sn clusters formed (independent of Cu) when the sample of Al−1.7at.%Cu−0.01at.%Sn alloy was quenched in water. These β-Sn particles have been thought to have a strong ability to act as the nucleation substrate for θ' phase ($I4/mmm$, a=0.404 nm, and c=0.580 nm [7]) with orientation relationships of $(001)_{\beta\text{-Sn}}//(001)_{\theta'}$ and $[110]_{\beta\text{-Sn}}//\ [100]_{\theta'}$ [16,26]. Thus, the formation of θ' phase can be promoted by the existence of Sn in Al−Cu alloy. The element mapping images in Fig. 6 indicate that there are some Sn-rich (β-Sn) particles existing inside/around θ' needle in the matrix of A4C−S alloy in T5 state. This favors the heterogeneous nucleation mechanism. The observation results in Fig. 2 demonstrate that Sn micro-alloying (0.019 wt.% Sn addition) in Al−4Cu alloy can accelerate the ageing precipitation process, namely, promote the formation of θ' precipitates. This will also lead to a variation in precipitation hardening effect.

4.2 Sn-induced mechanism of transformation from θ' to θ phase during LTHE treatment

During a long-time heat exposure process at high temperature, the ageing precipitates will

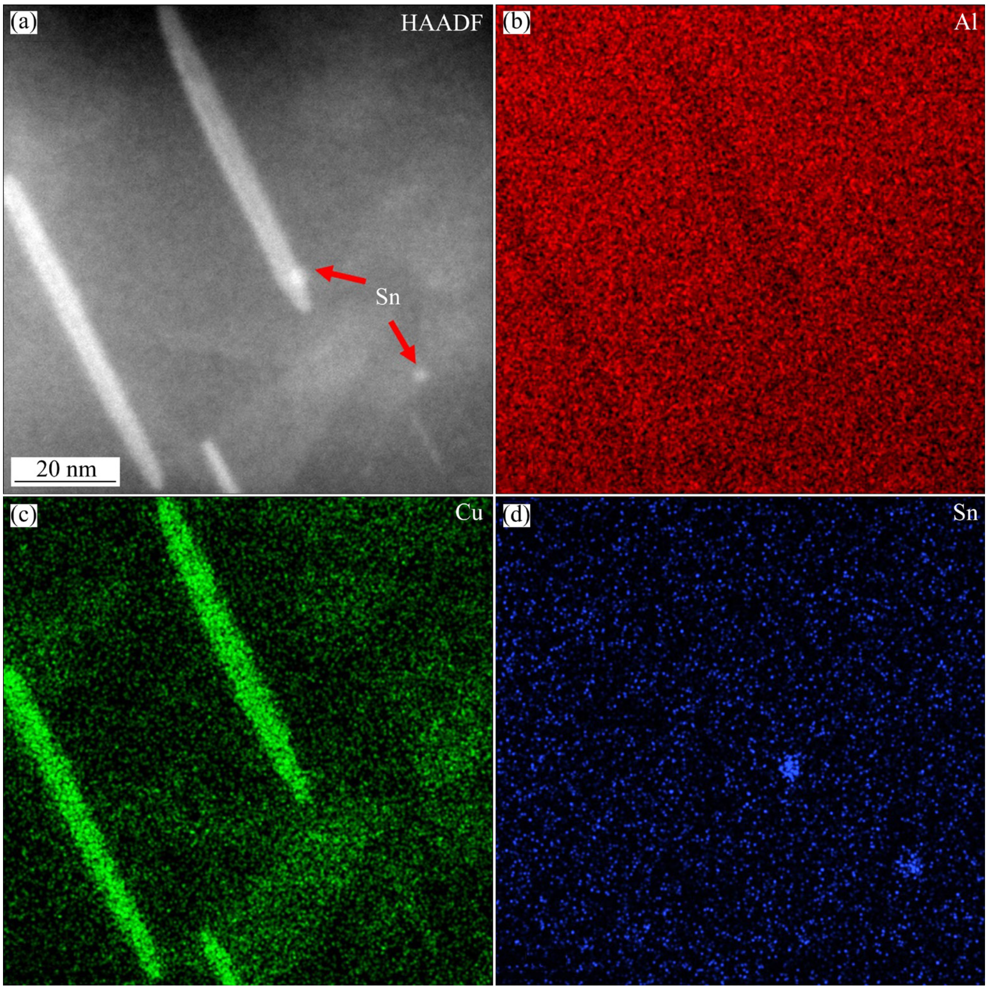

Fig. 6 HRTEM element mapping images of θ' needle in A4C−S alloy in T5 state, illustrating β-Sn particles acting as nucleation substrate for θ' phase

successively experience the phase transformation of $\theta''\rightarrow\theta'$, the coarsening of θ' phase, and the final phase transformation of $\theta'\rightarrow\theta$. As seen in Figs. 3 and 4, Sn addition induces different modes of $\theta'\rightarrow\theta$ phase transformation in Al−4Cu alloy after the LTHE treatment. It drives us to study the evolution of the ageing precipitates during heat exposure in details.

During the tensile test at 573 K, the samples in T5 state, first, must experience a holding time of 0.5 h at this temperature. It is equivalent to the STHE treatment (0.5 h). This state represents the beginning stage of the LTHE treatment. Thus, the variation of the ageing precipitates in this state stands for its evolution at the beginning stage of the LTHE treatment. Figure 7 illustrates TEM bright field images of ageing precipitates in the samples of A4C and A4C−S alloys (in T5 state) after the tensile test at 573 K and its SAED patterns. At the beginning stage (only after 0.5 h) of the LTHE treatment, all θ'' particles observed in T5 state, whether in A4C alloy or in A4C−S alloy, have transformed into θ' particles and they have been considerably coarsened too. However, the precipitation particles in A4C−S alloy (Sn micro-alloyed) are much smaller than those in A4C alloy as well as with a much higher number density. The reason for the refinement is the Sn-accelerated heterogeneous nucleation that has been discussed above.

Although there are a great number of research reports on the formation or transformation mechanisms of θ'' and θ' phases and on Sn-induced heterogeneous nucleation mechanism of θ', the mechanisms for $\theta'\rightarrow\theta$ phase transformation have not been well established. In this work, the process of $\theta'\rightarrow\theta$ phase transformation in Al−4Cu alloy is considered. As shown in Fig. 3, film-like θ phase forms along the surface of θ' needles. Element mapping images in Fig. 8 more definitely exhibit a sandwich structure, the same as that observed in Fig. 3(c). The proportion of Cu element in the

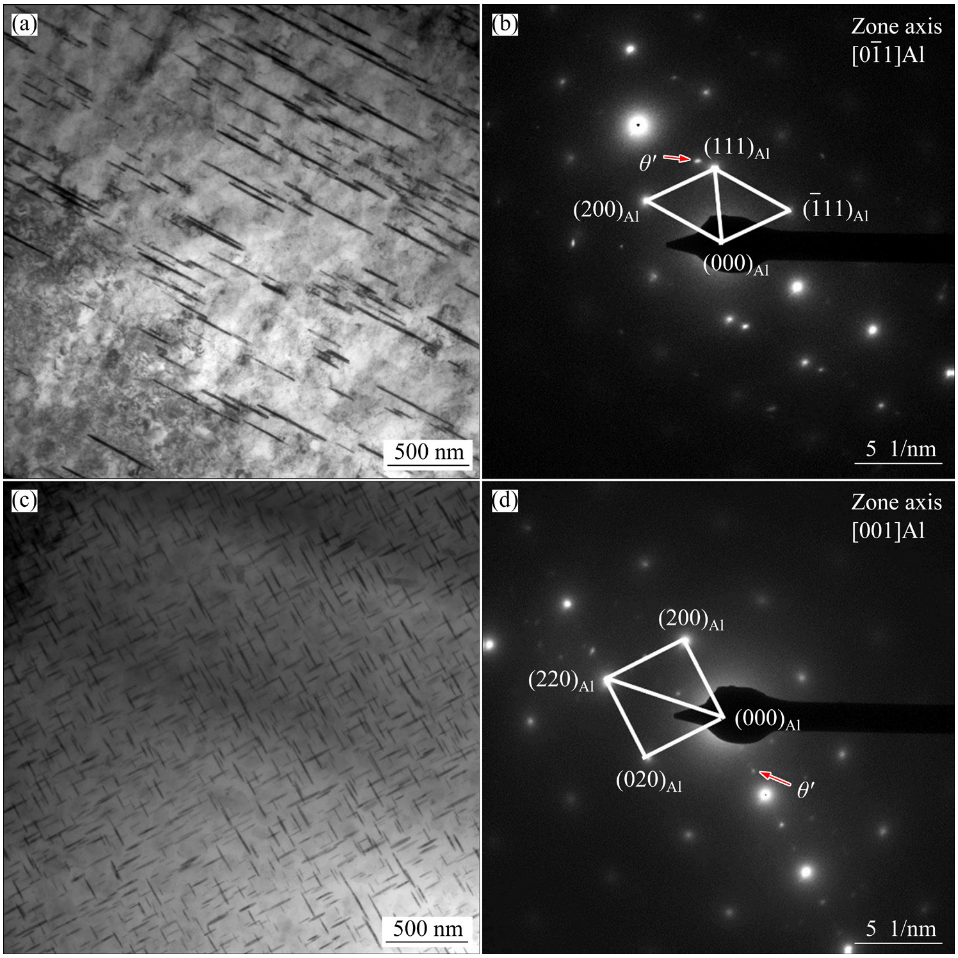

Fig. 7 TEM bright field images showing precipitates in matrix of A4C (a) and A4C−S (c) alloys in T5 state after tensile test at 573 K, and corresponding SAED patterns of zones containing precipitation particles for A4C (b) and A4C−S (d) alloys

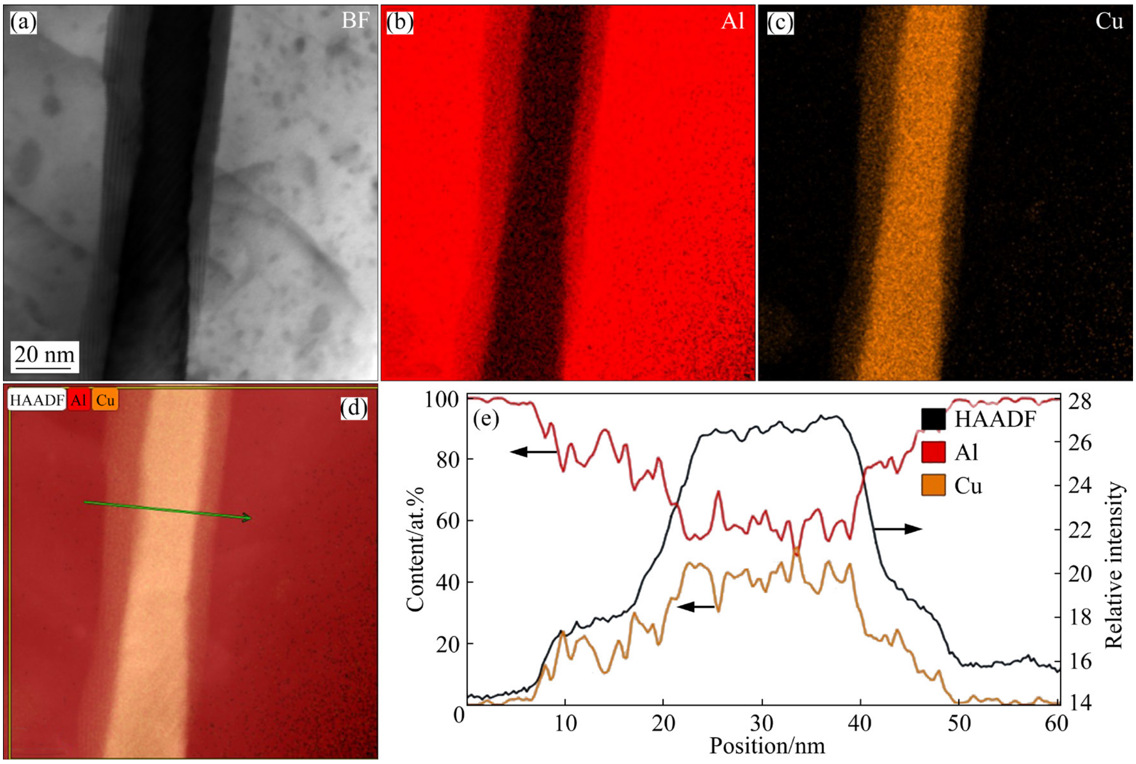

Fig. 8 Elements mapping images of precipitates with sandwich structure observed in A4C alloy in T5 state after LTHE treatment

inside is obviously higher than that in the outside and that of Al element is at the centre. Figures 3(d−f) demonstrate that the inside part is θ' phase and the outside part belongs to θ phase. This indicates that there is a phase transformation occuring on the surface of θ' particles by locally rearranging Cu atoms at the interface between the matrix and θ' phase. However, when focusing on the area marked by red frame in Figs. 9(a) and (b), it is found that there are some rod-like phases formed on the surface of the disc-like θ' phase (the coherent surface of θ' phase with α(Al) phase). Combining the observation in Fig. 3 and Fig. 8, it is thought that θ phase nucleates on the surface of the disc-like θ' phase and then grows in the form of rod along the surface through consuming the surrounding θ' phase. This transformation mechanism was observed in Al−4Cu wire (holding at 350 °C) by KAIRA et al [36] through synchrotron-based hard X-ray nanotomography technology. In our study, the sandwich structure observed through $[01\bar{1}]_{\mathrm{Al}}$ axis (shown in Fig. 3 and Fig. 8) is, in fact, the projection of the structure shown in Fig. 9(b). It is schematically illustrated in Fig. 9(c) with different axes of Al matrix.

However, for Sn micro-alloyed A4C−S alloy, there is not any connection observed between the short and small θ'-like rods and coarse θ needles, as shown in Fig. 4. It is also seen that θ phase grows in random directions, and seems to nucleate directly from the matrix. This indicates that the mechanism for $\theta'\rightarrow\theta$ phase transformation in A4C−S alloy during the LTHE treatment is quite different from that in A4C alloy. HAADF images in Figs. 10(a−d), which are obtained from different zones of the sample, suggest that many white particles are closely connected with θ phase. Elements mapping images of Cu and Sn elements shown in Figs. 10(e, f) clearly illustrate that these white particles are β-Sn phase adhered to the coarse needles of θ phase. Useful information about the orientation relationships between β-Sn and θ phase is not obtained by HRTEM. However, based on E2EM model [37−39], a good orientation relationship between θ and β-Sn phases is predicted: $(200)[010]_{\theta}//(200)[010]_{\beta\text{-Sn}}$ with f_{p}=3.9% and f_{d}= 3.8% (f_{p} is the plane mismatch degrees and f_{d} is the atom row mismatch degrees). HRTEM observation (Fig. 10) and E2EM prediction indicate that the pre-existed β-Sn particles can act as the efficient

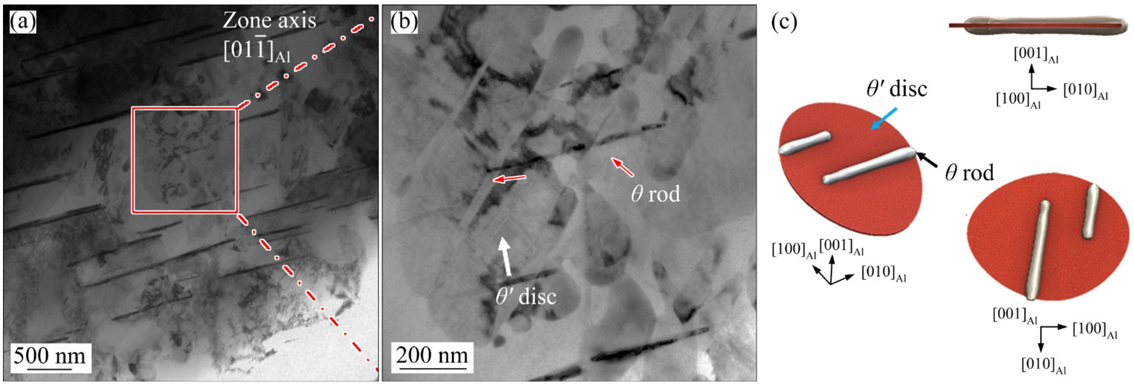

Fig. 9 TEM bright field images showing rod-like θ phase formed on disc-like surface of θ' phase in A4C alloy after LTHE treatment (a, b) and schematic diagram of sandwich structure observed in different axes (c)

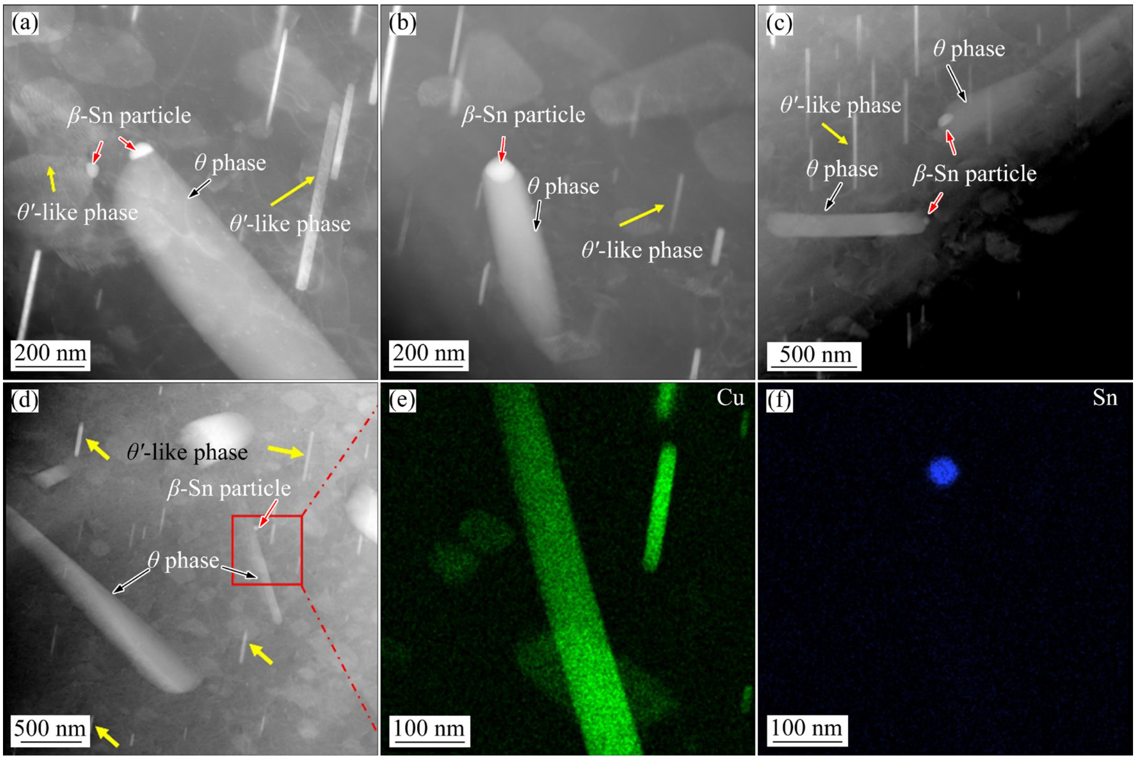

Fig. 10 HAADF images of precipitates obtained from different zones in A4C−S alloy in T5 state after LTHE treatment exhibiting many white particles connected with θ phase (a−d), and element mapping images of Cu (e) and Sn (f) elements suggesting β-Sn particle closely adhered to θ phase

heterogeneous nucleation substrates for θ phase and hence accelerate the phase transformation from θ' to θ (Fig. 4). Although the segregation of Sn at the interface of Al/θ' may affect the phase transformation from θ' to θ too, the segregation amount of Sn atoms is very few in the case of trace addition of Sn [16,35]. Thus, it is believed that the mechanism that θ phase heterogeneously nucleates on the pre-existed β-Sn particles dominates the phase transformation from θ' to θ during the LTHE treatment of A4C−S alloy.

So, it is reasonable to summarize the phase transformation mechanism from θ' to θ in A4C−S alloy during the LTHE treatment as: due to the existence of trace amount of Sn, there are many pre-formed β-Sn particles in the α(Al) solution (in T5 state of A4C−S alloy, β-Sn particles are also observed in Fig. 6); they can efficiently promote the formation of θ phase by acting as the heterogeneous nucleation substrates for it; thus, θ phase nucleates directly on β-Sn particles and grows in α(Al) solution at an expense of re-dissolution of the nearby or adjacent θ' particles. So, in A4C−S alloy after the LTHE treatment, many coarse needles of θ phase are formed with no specific orientations (seen in Fig. 4). At the same time, a larger number of θ' particles are re-dissolved into the matrix to provide Cu atoms for the growth of θ phase, and thus, the short and small θ'-like rod precipitates are observed in the matrix of A4C−S alloy (seen in Fig. 10).

The effect of trace addition of Sn to Al−4Cu alloy on the evolution of ageing precipitates can be schematically summarized in Fig. 11. During the designed solution, ageing treatments and short-time/long-time heat exposures (STHE/LTHE treatment), the evolution of ageing precipitates in A4C and A4C−S alloys can be described as: in T4 state, α(Al) solid solution is supersaturated for two alloys (schematically illustrated in Figs. 11(a) and (e)); in T5 state, all precipitates in A4C alloy are θ'' phase (Fig. 11(b)), but θ'' and θ' precipitates coexist in A4C−S alloy and the latter is dominant (Fig. 11(f)), where the prior existence of β-Sn particles accelerates the formation of θ' phase; in the state after STHE treatment, all precipitates in both A4C and A4C−S alloys are coarsened and become θ' phase, where the number density of precipitates in A4C−S alloy is much larger but the size is much smaller than those in A4C alloy (Figs. 11(c) and (g)); in the state after the LTHE treatment, θ' and θ precipitates coexist in both A4C and A4C−S alloys, where rod-like θ phase is formed on the coherent surface of the coarsened disc-like θ' phase in A4C alloy (Fig. 11(d)), and, in A4C−S alloy, coarse needles of θ phase nucleate directly on the pre-formed β-Sn particles in α(Al) solution and grow at the expense of the re-dissolution of nearby or adjacent θ' particles.

4.3 Effect of trace addition of Sn on variation of yield strength

The strength can be affected significantly by the microstructure evolution of ageing precipitates. In T5 state, the trace addition of Sn can significantly increase the yield strength from 159 to 283 MPa at room temperature. It is because the existence of trace amount of Sn accelerates the formation of θ' phase. In A4C alloy, when encountering with the oncoming dislocations, θ'' precipitates can be easily cut off in rows by dislocations, because the thickness of them is too small (only about 1 nm). The resistance of these fine θ'' precipitation particles to dislocation motion is small [3]. However, θ' and θ'' precipitates in the A4C−S alloy are thick and strong enough (about 4 and 2 nm in thickness, respectively) so that the dislocations cannot cut them off in rows, thus, dislocation-bypass mechanism is dominant [40]. This will cause a significant precipitation hardening effect. It is also the reason for that the peak hardening effect usually emerges when $\theta''+\theta'$ coexist in Al−Cu alloy or $\beta''+\beta'$ precipitates coexist in Al−Si−Mg alloy. After the same ageing treatment, the precipitates in A4C alloy are fine θ'' particles with a very small thickness (Fig. 2(a)); however, in A4C−S alloy, the relatively

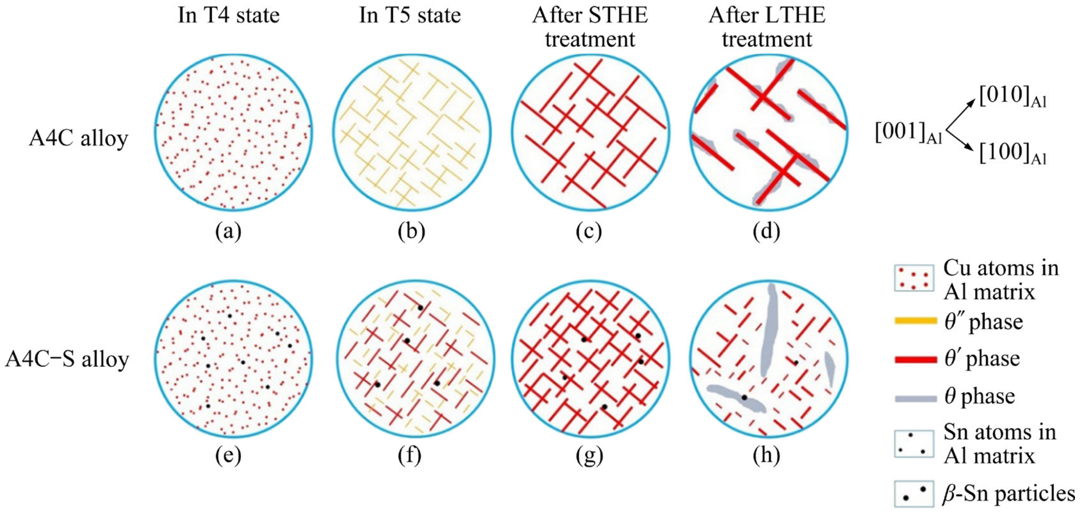

Fig. 11 Schematic model illustrating effect of trace addition of Sn on evolution of ageing precipitates in different alloys in different states: (a−d) A4C alloy; (e−h) A4C−S alloy

coarse precipitates of $\theta''+\theta'$ phases coexist (Fig. 2(c)). Trace addition of Sn accelerates the ageing precipitation process. Therefore, the room temperature yield strength of A4C−S alloy is much higher than that of A4C alloy (more than about 124 MPa).

Before the stress is loaded to the testing samples, samples for the tensile test at 573 K must be held at this temperature for 0.5 h to homogenize the temperature. This is equivalent to a STHE treatment. Surely, the ageing precipitates will evolve even during this short-time history at 573 K. Respectively, Figs. 7(a) and (c) show that the microstructure evolutions have occurred in A4C and A4C−S alloys in T5 state after the tensile test at 573 K, respectively. Compared Figs. 7(a) and (c) with Figs. 2(a) and (c), it is seen that the precipitation particles in the matrix of both A4C and A4C−S alloys have been greatly coarsened after this short-time history at 573 K. Compared Fig. 7(c) with Fig. 7(a), it is also found that the number density of θ' precipitation particles in A4C−S alloy after the tensile test at 573 K is much greater than that in A4C alloy but the size is much smaller either. TEM/HRTEM observations in the samples of A4C and A4C−S alloys confirm that the formation of θ' phase during the ageing treatment course can be accelerated by the existence of β-Sn particles (Figs. (2) and (6)). During the phase transformation of $\theta''\rightarrow\theta'$ in the course of tensile test at 573 K, the existence of Sn plays the same role, that is, Sn in the A4C−S alloy can significantly increase the nucleation rate of θ' phase. Thus, the number density of θ' precipitates in A4C−S alloy after the tensile test at 573 K is much higher than that in A4C alloy and the size is much smaller (Fig. 7). Because the duration from applying the stress on the samples to fracture in the course of high temperature tensile test is always less than 5 min, the microstructure of the samples after the tensile test at 573 K is approximately equivalent to the microstructure before the stress starts applying. The precipitation particles in A4C−S alloy with a higher number density and a smaller size make the matrix have a stronger resistance to dislocation motions. Thus, $\sigma_{0.2}$ of A4C−S alloy at 573 K (130 MPa) is much higher than that of A4C alloy (93 MPa).

After the LTHE treatment, the formation of θ phase on the surface of θ' phase and further coarsening of θ' phase in A4C alloy result in a considerable decrement in the yield strength at 573 K, from 93 to 74 MPa, as shown in Table 1. For A4C−S alloy after the same LTHE treatment, the formation of coarse needle-like θ phase is obviously observed, but the coarsening of θ' phase is not observed. Conversely, smaller and shorter θ'-like particles are observed (shown in Fig. 4(a)). The phase transformation from θ' to θ will lead to a loss in strength. However, because there are still a high proportion of fine θ'-like rods, the decrement in $\sigma_{0.2}$ at 573 K from the LTHE treatment is expected to be small. But, in fact, it is very large, from 130 to 63 MPa. This drives us to further study the strengthening effect of these short and small θ'-like rods. As described above, these short and small θ'-like rods observed in A4C−S alloy are not the normal θ' precipitates, but a variant of θ' phase (Fig. 4). Though these θ'-like rods have a small size and a high proportion, it is in doubt that they have the same strengthening effect as the normal θ' precipitates. The bright/dark field TEM images in Figs. 12(a−c) exhibit that there are some dislocations cutting through these θ'-like rods, obtained in the A4C−S alloy in the LTHE state after the tensile test at 573 K. HRTEM images in Figs. 12(d−f) reveal the evidences for the dislocation-cutting mechanism. This indicates that these short and small θ'-like rods have little resistance to dislocation motion as the normal θ' particles. It is related to the small thickness and structure instability of these rods. The redissolving of θ' phase during the phase transformation from θ' to θ in A4C−S alloy has destroyed the perfectness and compactness of normal θ' phase and thus it becomes a variant that has little resistance to dislocation motion. It is known that the coarse precipitation particles of θ phase have little contribution to the strengthening of matrix [23]. Therefore, for A4C−S alloy in T5 state after the LTHE treatment, $\sigma_{0.2}$ at 573 K is greatly decreased by 52%. However, for AC4 alloy in T5 state after the same LTHE treatment, the decrement in $\sigma_{0.2}$ at 573 K is only 20%. This difference is due to different phase transformation mechanisms of $\theta'\rightarrow\theta$ during the LTHE treatment. The trace addition of Sn to Al−4Cu alloy accelerates the phase transformation of $\theta'\rightarrow\theta$ during the LTHE treatment, which results in a significant degradation in the yield strength at 573 K. Two suggestions for high temperature application of Al−Cu system alloy

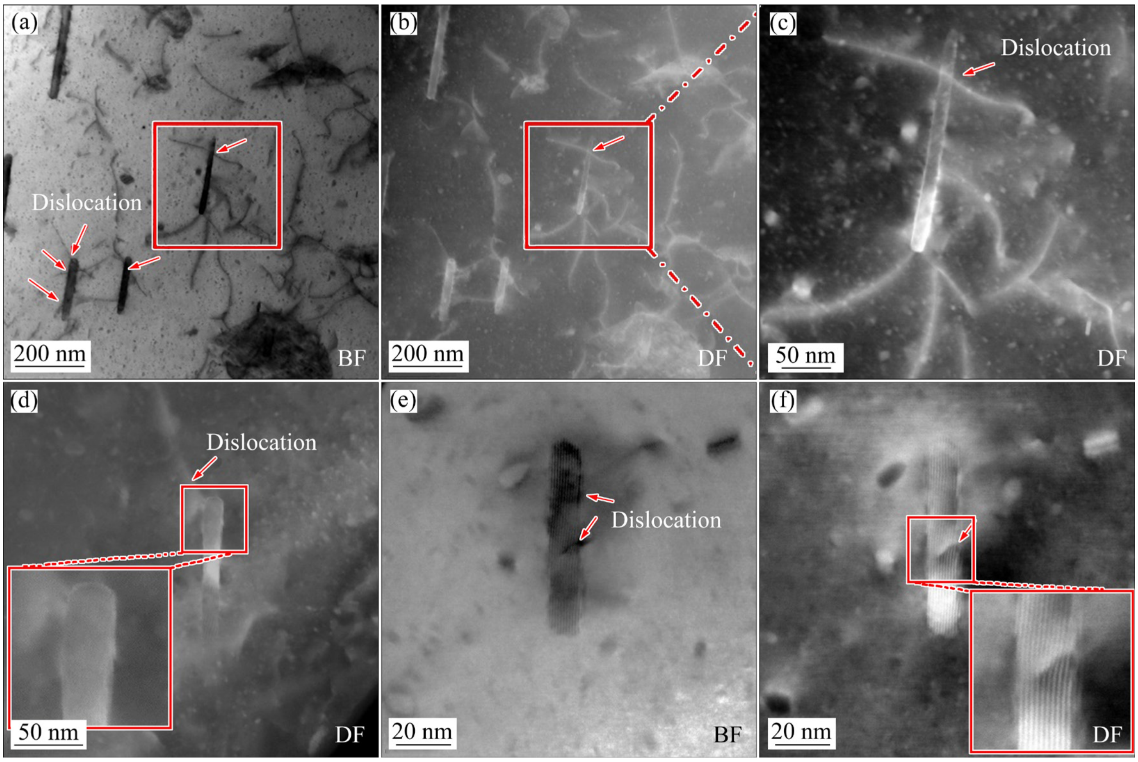

Fig. 12 TEM images showing dislocations cutting through θ'-like particles in A4C−S alloy in LTHE state after tensile test at 573 K (a−c) and HRTEM images revealing cutting traces in rods by dislocations (d−f)

could be obtained from this study. One is that the phase transformation from θ' to θ through θ directly nucleating in the solution and growing by re-dissolving θ' phase should be avoided. The other is that impurity Sn in Al−Cu system alloy should be removed as much as possible.

5 Conclusions

(1) 0.02 wt.% addition of Sn to Al−4Cu alloy leads to completely different mechanisms for $\theta'\rightarrow\theta$ phase transformation during the long-time heat exposure at 573 K for 100 h. In the alloy without Sn micro-alloying, it is found that rod-like θ phase is formed along the coherent surface of coarsened θ' phase. However, in the alloy with Sn-micro-alloying, θ phase first heterogeneously nucleates on pre-formed β-Sn particles, then grows by re-dissolving the nearby or adjacent θ' particles, and finally becomes much coarse needle-like θ phase.

(2) Sn micro-alloying can accelerate the formation of θ' phase in T5 state, and also leads to a significant increase in the number density of θ' phase and a great decrease in its size during the short-time heat exposure at 573 K for 0.5 h. Thus, Sn micro-alloying in Al−4Cu alloy can significantly increase the yield strength ($\sigma_{0.2}$) in T5 state at both room temperature and 573 K.

(3) It is Sn-induced mechanism for $\theta'\rightarrow\theta$ phase transformation that results in the greater decrease in $\sigma_{0.2}$ at 573 K of the Al−4Cu−0.02Sn alloy after the long-time heat exposure at 573 K for 100 h than that of the Al−4Cu alloy.

(4) For high temperature application of Al−Cu system alloy, the phase transformation of from θ' to θ through θ directly nucleating in the solution and growing by re-dissolving θ' phase should be avoided, and impurity Sn in Al−Cu system alloy should be removed as much as possible.

Acknowledgments

This work is supported by Jiangsu Key Laboratory for Advanced Metallic Materials, China (No. BM2007204), and the Fundamental Research Funds for the Central Universities, China (No. 2242016k40011).

References

[1] DENG Yun-lai, ZHANG Xin-ming. Development of

aluminium and aluminium alloy [J]. The Chinese Journal of Nonferrous Metals, 2019, 29(9): 2115−2141. (in Chinese)

[2] ANDERSEN S J, MARIOARA C D, FRIIS J, WENNER S, HOLMESTAD R. Precipitates in aluminium alloys [J]. Advances in Physics: X, 2018, 3: 790−813.

[3] BELLÓN B, HAOUALA S, LLORCA J. An analysis of the influence of the precipitate type on the mechanical behavior of Al−Cu alloys by means of micropillar compression tests [J]. Acta Materialia, 2020, 194: 207−223.

[4] TSAO C S, HUANG E W, WEN M H, KUO T Y, JENG S L, JENG U S, SUN Y S. Phase transformation and precipitation of an Al−Cu alloy during non-isothermal heating studied by in situ small-angle and wide-angle scattering[J]. Journal of Alloys and Compounds, 2013, 579: 138−146.

[5] RAKHMONOV J, LIU K, CHEN G X. Effects of compositional variation on the thermal stability of θ'-Al$_2$Cu precipitates and elevated-temperature strengths in Al−Cu 206 alloys [J]. Journal of Materials Engineering and Performance, 2020, 29: 7221−7230.

[6] LIU L, CHEN J H, WANG S B, LIU C H, YANG S S, WU C L. The effect of Si on precipitation in Al−Cu−Mg alloy with a high Cu/Mg ratio [J]. Materials Science and Engineering: A, 2014, 606: 187−195.

[7] BASTOW T J, CELOTTO S. Structure evolution in dilute Al(Cu) alloys observed by ^{63}Cu NMR [J]. Acta Materialia, 2003, 51: 4621−4630.

[8] SUN Dong-qiang, WANG Yong-xin, ZHANG Xin-yi, ZHANG Min-yu, NIU Yan-fei. First-principles calculation on the thermodynamic and elastic properties of precipitations in Al−Cu alloys [J]. Superlattices and Microstructures, 2016, 100: 112−119.

[9] ZHANG Y, ZHANG Z, MEDHEKAR N V, BOURGEOIS L. Vacancy-tuned precipitation pathways in Al−1.7Cu−0.025In−0.025Sb (at.%) alloy [J]. Acta materialia, 2017, 141: 341−351.

[10] SHOWER P, POPLAWSKY J, BAHL S, SHYAM A. The role of Si in determining the stability of the θ' precipitate in Al−Cu−Mn−Zr alloys [J]. Journal of Alloys and Compounds, 2021, 862: 158152.

[11] HEUGUE P, LAROUCHE D, BRETON F, MARTINEZ R, CHEN X G. Evaluation of the growth kinetics of θ' and θ-Al$_2$Cu precipitates in a binary Al−3.5 wt pct Cu alloy [J]. Metallurgical and Materials Transactions A, 2019, 50: 3048−3060.

[12] BOURGEOIS L, DWYER C, WEYLAND M, NIE J F, MUDDLE B C. Muddle, structure and energetics of the coherent interface between the θ' precipitate phase and aluminium in Al−Cu [J]. Acta Materialia, 2011, 59: 7043−7050.

[13] BOURGEOIS L, ZHANG Y, ZHANG Z, CHEN Y, MEDHEKAR N V. Transforming solid-state precipitates via excess vacancies [J]. Nature Communications, 2020, 11: 1248.

[14] GAO Lin, LI Kai, NI Song, DU Yong, SONG Min. The growth mechanisms of θ' precipitate phase in an Al−Cu alloy during aging treatment [J]. Journal of Materials Science & Technology, 2021, 61: 25−32.

[15] DORIN T, RAMAJAYAM M, LAMB J, LANGAN T. Effect of Sc and Zr additions on the microstructure/strength of Al−Cu binary alloys [J]. Materials Science and Engineering: A, 2017, 707: 58−64.

[16] WANG R H, WEN Y, CHEN B A. Sn microalloying Al−Cu alloys with enhanced fracture toughness [J]. Materials Science and Engineering: A, 2021, 814: 141243.

[17] SATO T, TAKAHASHI T. High resolution electron microscopy studies on the precipitation in an Al−4%Cu alloy [J]. Transactions of the Japan Institute of Metals, 1983, 24(6): 386−395.

[18] HEADLEY T, HREN J. Characterization and mechanism of repeated precipitation on dislocations in an Al−Cu alloy [J]. Philosophical Magazine, 1976, 34(1): 101−117.

[19] BOURGEOIS L, MEDHEKAR N V, SMITH A E, WEYLAND M, NIE J F, CHRISTIAN D. Efficient atomic-scale kinetics through a complex heterophase interface [J]. Physical Review Letters, 2013, 111(4): 046102.

[20] RAKHMONOV J, LIU K, PAN L, BRETON F, CHEN X G. Enhanced mechanical properties of high-temperature-resistant Al−Cu cast alloy by microalloying with Mg [J]. Journal of Alloys and Compounds, 2020, 827: 154305.

[21] SUN Teng-teng, GENG Ji-wei, BIAN Ze-yu, WU Yi, WANG Ming-liang, CHEN Dong, MA Nai-heng, WANG Hao-wei. Enhanced thermal stability and mechanical properties of high-temperature resistant Al−Cu alloy with Zr and Mn micro-alloying [J]. Transactions of Nonferrous Metals Society of China, 2022, 32: 64−78.

[22] POPLAWSKY J D, MILLIGAN B K, ALLARD L F, SHIN D, SHOWER P, CHISHOLM M F, SHYAM A. The synergistic role of Mn and Zr/Ti in producing θ'/L1$_2$ co-precipitates in Al−Cu alloys [J]. Acta Materialia, 2020, 194: 577−586.

[23] SHYAM A, ROY S, SHIN D, POPLAWSKY J D, ALLARD L F, YAMAMOTO Y, MORRIS J R, MAZUMDER B, IDROBO J C, RODRIGUEZ A, WATKINS T R, HAYNES J A. Elevated temperature microstructural stability in cast AlCuMnZr alloys through solute segregation [J]. Materials Science and Engineering: A, 2019, 765: 138279.

[24] SULLY A H, HARDY H K, HEAL T J. The aluminum−tin phase diagram and the characteristics of aluminum alloys containing tin as an alloying element [J]. The Journal of the Institute of Metals, 1949, 76: 269−294.

[25] WOLCYRZ M, KUBIAK R, MACIEJEWSKI S. X-ray investigation of thermal expansion and atomic thermal vibrations of tin, indium, and their alloys [J]. Physica Status Solidi (b), 1981, 107: 245−253.

[26] BOURGEOIS L, DWYER C, WEYLAND M, NIE J F, MUDDLE B C. The magic thicknesses of θ' precipitates in Sn-microalloyed Al−Cu [J]. Acta Materialia, 2012, 60: 633−644.

[27] HE Chuan, LUO Bing-hui, ZHENG Ya-ya, YIN Yuan, BAI Zhen-hai, REN Zhi-wei. Effect of Sn on microstructure and corrosion behaviors of Al−Mg−Si alloys [J]. Materials Characterization, 2019, 156: 109836.

[28] LI Guang-jing, LIAO Heng-cheng, ZHENG Ji-wei, CHEN hao, LU Li-zhen, YANG Lin-long, GUO Hui-ting. Micro-alloying effects of Mn and Zr on the evolution of ageing precipitates and high temperature strength of Al−11.5Si−4Cu alloy after a long-time heat exposure [J].

Materials Science and Engineering: A, 2021, 828: 142121.

[29] LI Guang-jing, LIAO Heng-cheng, XU Ai-qun, TANG Jing-fan, ZHAO Bao-jun. Peritectic reaction between two primary Mn-rich phases during solidification of Al−Si−Cu−Mn heat-resistant alloy and the effect of cooling rate on it [J]. Journal of Alloys and Compounds, 2018, 753: 239−246.

[30] MONDOL S, MAKINENI S K, KUMAR S, CHATTOPADHYAY K. Enhancement of high temperature strength of 2219 alloys through small additions of Nb and Zr and a novel heat treatment [J]. Metallurgical and Materials Transactions A, 2018, 49: 3047−3057.

[31] SHEN Zhen-ju, DING Qing-qing, LI Chun-hui, WANG Jiang-wei, HE Tian, LI Ji-xue, ZHANG Ze. Atomic-scale mechanism of the $\theta'' \rightarrow \theta'$ phase transformation in Al−Cu alloys [J]. Journal of Materials Science & Technology, 2017, 33: 1159−1164.

[32] PORTER D A, EASTERLING K E, SHERIF M Y. Phase transformations in metals and alloys [M]. 3rd ed. Boca Raton: CRC Press, 2004: 293.

[33] PENG J, BAHL S, SHYAM A, HAYNES J A, SHIN D. Solute-vacancy clustering in aluminum [J]. Acta Materialia, 2020, 196: 747−758.

[34] NING Fang, ZOU Chun-ming, WEI Zun-jie, WANG Hong-wei, ZHANG Xue-jian, TAO Chang. Effect of Ge and Mg additions on the aging response behavior and mechanical properties of Al−Si−Cu alloy [J]. Materials Science and Engineering: A, 2021, 811: 141024.

[35] HOMMA T, MOODY M P, SAXEY D W, RINGER S P. Effect of Sn addition in precipitation stage in Al−Cu alloys: A correlative transmission electron microscopy and atom probe tomography study [J]. Metallurgical & Materials Transactions A, 2012, 43: 2192−2202.

[36] KAIRA C S, ANDRADE V D, SUDHANSHU S S, KANTZOS C, KIRUBANANDHAM A, CARLO F D, CHAWLA N. Probing novel microstructural evolution mechanisms in aluminum alloys using 4D nanoscale characterization [J]. Advanced Materials, 2017, 29: 1703482.

[37] ZHANG M X, KELLY P M, EASTON M A, TAYLOR J A. Crystallographic study of grain refinement in aluminum alloys using the edge-to-edge matching model [J]. Acta Materialia, 2005, 53: 1427−1438.

[38] ZHANG M X, KELLY P M, QIAN M, TAYLOR J A. Crystallography of grain refinement in Mg–Al based alloys [J]. Acta materialia, 2005, 53: 3261−3270.

[39] JING Li-jun, PAN Ye, LU Tao, PI Jing-hong, GU Teng-fei. Nucleation potency prediction of LaB_6 with E2EM model and its influence on microstructure and tensile properties of Al−7Si−0.3 Mg alloy [J]. Transactions of Nonferrous Metals Society of China, 2018, 28(9): 1687−1694.

[40] GONG Yan-li, GAO Lin, LI Kai, DU Yong, SONG Min. Structural instability of plate-shaped θ' precipitates in an aged Al−Cu alloy [J]. Philosophical Magazine Letters, 2020, 100: 524−532.

Sn 诱导 Al−4Cu 合金中 θ'相向 θ 相的相转变机制及其对合金高温强度的影响

李广敬，潘星惠，廖恒成，郑基伟，杨墨瞳，钱龙杰，陆丽珍

东南大学 材料科学与工程学院 江苏省先进金属材料高技术研究重点实验室，南京 211189

摘　要：通过显微组织观察和拉伸试验研究添加 0.02%Sn(质量分数)对 Al−4Cu 合金在 573 K 高温热暴露过程(100 h)中 θ'向 θ 相转变机制和高温强度的影响。研究结果表明，Sn 微合金化能完全改变 Al−4Cu 合金在持久热暴露过程中 θ'相向 θ 相的相转变机制。在未添加 Sn 的 Al−4Cu 合金中，棒状 θ 相在粗化后的盘状 θ'相的表面形核和生长。然而，当添加少量 Sn 后，θ 相首先在 β-Sn 颗粒上异质形核，然后形成粗大的针状相。由于 Sn 微合金化能提高 Al−4Cu 合金中 θ'相的数密度并降低其尺寸，因此，Al−4Cu 合金在 T5 状态下的室温和 573 K 高温下的屈服强度得到显著提高。然而，Sn 微合金化能同时促进持久热暴露过程中 θ'相向 θ 相的转变，导致 Al−4Cu 合金在热暴露后的高温(573 K)强度显著降低。

关键词：锡；Al−Cu 合金；θ 相；持久热暴露；相转变；高温强度

(Edited by Wei-ping CHEN)